

Petrology of lherzolite xenoliths of Hosséré Sédé volcano (Adamawa plateau, Ngaoundéré area, Cameroon)

O. F. Nkouandou¹ · J. M. Bardintzeff² · Fagny Mefire¹ · Njankouo Ndassa¹ · A. A. Sahabo³ · H. Adama¹

Received: 21 November 2022 / Revised: 22 May 2023 / Accepted: 2 June 2023 / Published online: 24 June 2023
© The Author(s), under exclusive licence to Science Press and Institute of Geochemistry, CAS and Springer-Verlag GmbH Germany, part of Springer Nature 2023

Abstract Numerous mantle xenoliths 6–12 cm in size and sub-angular to rounded in shape occur within Mio-Pliocene basanite lavas of the monogenetic volcano of Hosséré Sédé in the Adamawa plateau. Xenoliths of spinel lherzolite exhibit protogranular, equigranular or porphyroclastic texture. Microprobe chemical analyses show that olivine is highly magnesian ($Fo_{88.90}$), clinopyroxene crystals are diopside and augite ($Wo_{41.6-49.6} En_{45.3-53.7} Fs_{4.2-6.2}$), orthopyroxene crystals are enstatite ($Wo_{1.4-1.5} En_{88.6-89.0} Fs_{9.6-9.9}$) and spinel crystals are mainly Al-spinel associated to minor Cr-spinel. Estimated temperatures and pressures through empirical formulas show that Hosséré Sédé xenoliths have equilibrated between 1085 and 1204 °C and 1.08 to 1.57 GPa, corresponding to sampling depths of 36 and 52 km. Detailed petrographical and mineral chemistry of Hosséré Sédé xenoliths evidences the complex nature and composition of the subcontinental lithosphere under the Adamawa plateau. This may involve a probable uplift of the whole area after a limited extensional event, possible metasomatism through melt infiltration during shearing of the lithospheric mantle along the Pan African strike-slip fault system.

Keywords Cameroon · Adamawa · Hosséré Sédé · Subcontinental lithosphere · Xenolith · Peridotite · Lherzolite

1 Introduction

Cameroon Volcanic Line, Benue Through and Adamawa plateau are major tectono-volcanic structures in central Africa (Fig. 1A and B). The alignment of volcanoes on the Cameroon Volcanic Line has been interpreted as the result of the locally weakened continental crust due to inherited discontinuities from the Pan African orogeny and reactivated during Mesozoic and Cenozoic times (Moreau et al. 1987; Fagny et al. 2016, 2020).

The nature and composition of sub-continental lithospheric mantle under those structures are rather well documented. The mechanical behavior and the relationships between tectonic features and rigidity of the subcontinental lithosphere under the Cameroon Volcanic Line and Adamawa plateau were investigated, using gravity data (Poudjom Djomani et al. 1992, 1995), and magnetic data for Benue Trough (Ofoegbu 1984; Shemang et al. 2001).

The continental crust of the Adamawa plateau is about 30 km thick (Poudjom Djomani et al. 1995; Nnange et al. 2000; Goussi Ngalamo et al. 2017), and likely thinner in its northern part where the ascent of magma was facilitated by Pan African strike-slip faults straddling crust and subcontinental mantle down to asthenosphere (Dorbath et al. 1986). Cenozoic uplift of the Adamawa plateau might have been associated with the upwelling of the underlying mantle, which underwent decompression-induced melting (Nkouandou et al. 2008, 2010, 2015; Njankouo Ndassa

✉ J. M. Bardintzeff
jacques-marie.bardintzeff@universite-paris-saclay.fr

¹ Department of Earth Sciences, Faculty of Sciences, University of Ngaoundéré, P.O. Box. 454, Ngaoundéré, Cameroon

² Univ Paris-Saclay, Sciences de la Terre, Volcanologie-Planétopologie, UMR CNRS 8148 GEOPS, Bât. 504, 91405 Orsay, France

³ Laboratoire de volcanologie, Institut de Recherches Géologique et Minière, B.P. 370, Buea, Cameroon

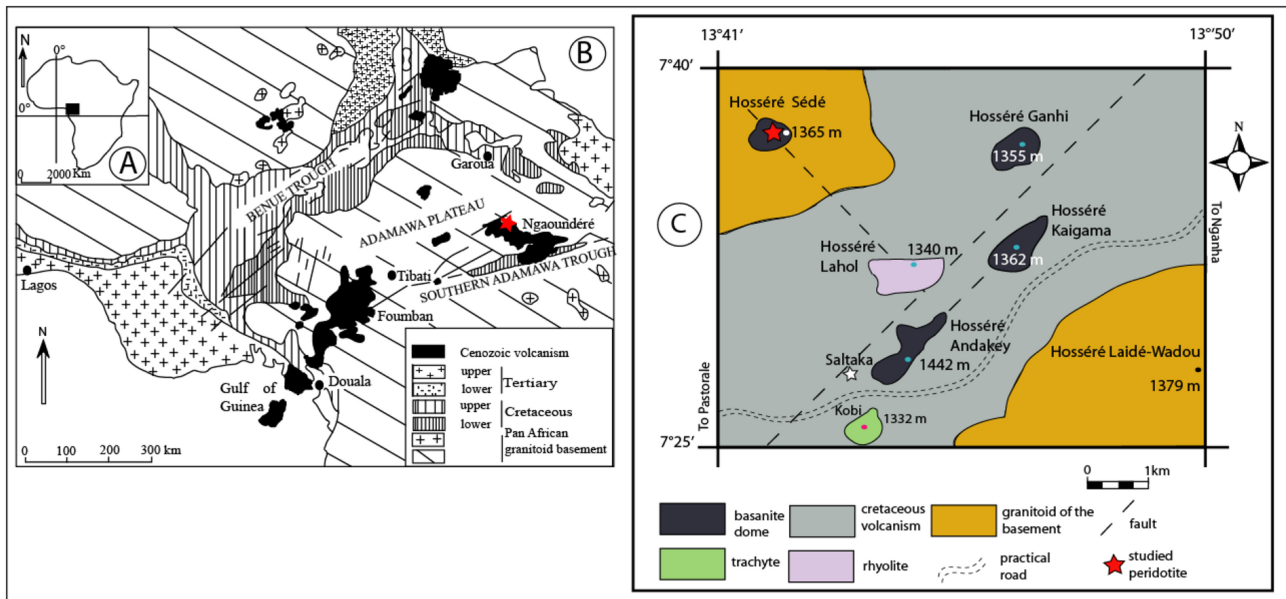


Fig. 1 **A** Location in Africa, **B** Main tectono-magmatic structures in Cameroon, modified after Dumont (1987), in black is the Cenozoic volcanism of the Cameroon Volcanic Line, red star=studied area, **C** Geological sketch map of Saltaka–Hossé Séde area

et al. 2019). Sub-continental peridotite fragments sampled by ascending basaltic magmas on their way to the surface have certainly recorded mechanical markers and composition of the lithospheric mantle under the Adamawa plateau.

Peridotite xenoliths that we recently discovered in Hossé Séde volcano, north of Ngaoundéré in the Adamawa plateau (Fig. 1C) could offer more information on the structure and composition of the underlying lithospheric mantle.

This work aims to obtain precise data on the chemistry of the mineral phases constituting the xenoliths and to calculate the temperature and pressure conditions of their formations at depth for a better knowledge of the lithosphere in this area.

2 Geological setting

Adamawa plateau in central Cameroon is a volcanic and tectonic dome structure within the Pan-African belt of Cameroon (Fig. 1B). It is covered by 11–7 Ma basaltic and felsic volcanic formations (Temdjam et al. 2004; Nkoudou et al. 2008). Its basement is composed mostly of 630–620 Ma pre- to syn-D1, 580–600 Ma syn-D2, and 550 Ma post-orogenic granitoid (Toteu et al. 1987, 2001; Toteu 1990). Neoarchean to Paleoproterozoic pyroxene-and amphibole-bearing gneisses located south of Meiganga display geochemical characteristics of Archean TTG (tonalite—trondhjemite—granodiorite) and yield $^{207}\text{Pb}/^{206}\text{Pb}$ single-zircon evaporation ages of 2.6–1.7 Ga

(Ganwa et al. 2008). Adamawa plateau is bounded north and south by Pan African strike-slip faults, the reactivation of which has favored Cenozoic uplift (Ngangom 1983; Dumont 1987; Moreau et al. 1987). Geophysical studies on the Adamawa plateau (Poudjom Djomani et al. 1992, 1995, 1997; Nnange et al. 2000, 2001) identify broad negative and central positive Bouguer anomalies deduced from the Bouguer anomaly map of Cameroun corresponding to lithospheric and crustal thinning, respectively. Four major density discontinuities have been determined within the lithosphere beneath the Adamawa uplift using spectral analysis of gravity data (Nnange et al. 2000): (1) the first discontinuity is located between 7 ± 0.5 and 13 ± 1 km; (2) between 19 ± 1 and 25 ± 4 km; (3) between 30 ± 2 and 37 ± 2 km and (4) 75 ± 10 and 149 ± 27 km. The deepest discontinuity depths suggest the presence of an anomalous low-velocity upper mantle structure, already deduced from teleseismic delay time studies (Poudjom Djomani et al. 1992). The 30–37 km depths correspond to Moho's average depth of 33 km below the Benue trough and Adamawa dome and the intermediate depths of 10 and 20 km obtained may correspond to intracrustal discontinuities.

3 Materials and methods

Sampled peridotites recently discovered in Hossé Séde volcano were studied for petrography using 5 thin sections prepared at the laboratory GEOPS (GEO sciences Paris-Saclay), University Paris-Saclay, France. Modal

proportions of the four major mineral phases (olivine, clinopyroxene, orthopyroxene, and spinel) of studied lherzolite peridotites selected for this work have been estimated from percentage areas of each crystal under the polarizing microscope and Scanning Electron Microscope (SEM) in the laboratory GEOPS, University Paris-Saclay, France. Microprobe mineral analyses of ultramafic xenoliths were performed on Camebax SX100 at the service Camparis of the University Paris-Sorbonne, France. The operating conditions were accelerating voltage and beam current as follows: olivine and pyroxene: 15 kV and 40 nA, 20 s except Si for olivine (10 s) and Ti for pyroxene (30 s); titanomagnetite: 15 kV and 40 nA, Si, Ca, Ni: 10 s; Mn: 25 s; Cr: 15 s; Al: 30 s; Ti, Fe, Mg: 40 s. The standard used was a combination of natural and synthetic minerals. Data corrections were made using the PAP correction of Pouchochou and Pichoir (1991).

Table 1 GPS coordinates of Hosséré Séde xenolith samples

Sample	Latitude (N)	Longitude (E)	Altitude (m)	Precision (m)
A36	07°39'10.5"	13°41'8"	1251	3
S20	07°39'08.9"	13°41'41.5"	1278	3
F12	07°39'06.3"	13°41'36.1"	1365	3



Fig. 2 **A** Panoramic view of Hosséré Séde volcano, **B** Vesicular structure of basaltic block lava, **C** Angular peridotite xenolith enclosed in basalt

4 Results

4.1 Field-work and petrography

Studied peridotites have been sampled at the right hillside and top of Hosséré Séde volcano located 7°39' N and 13°41' E (Fig. 1C, Table 1), 4 km NNW of Saltaka and 35–40 km N of Ngaoundéré. The volcano, culminating at

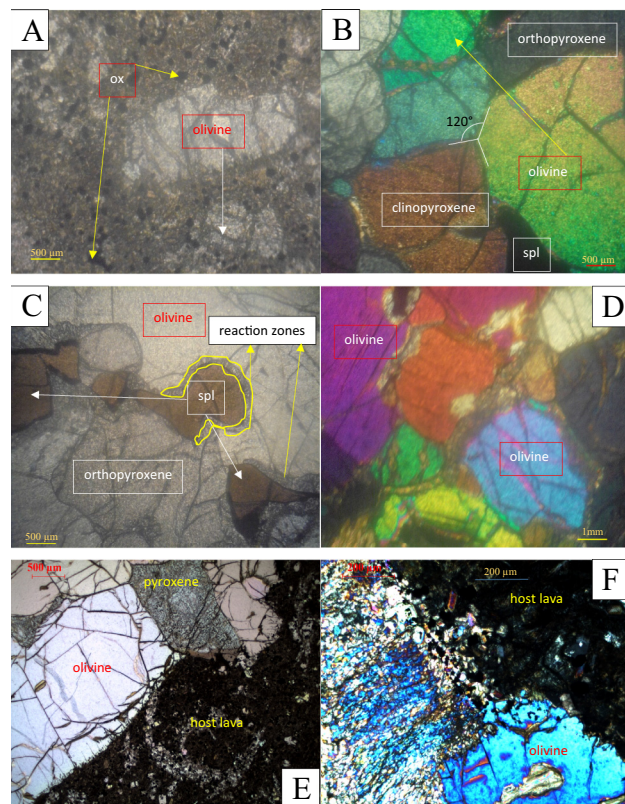
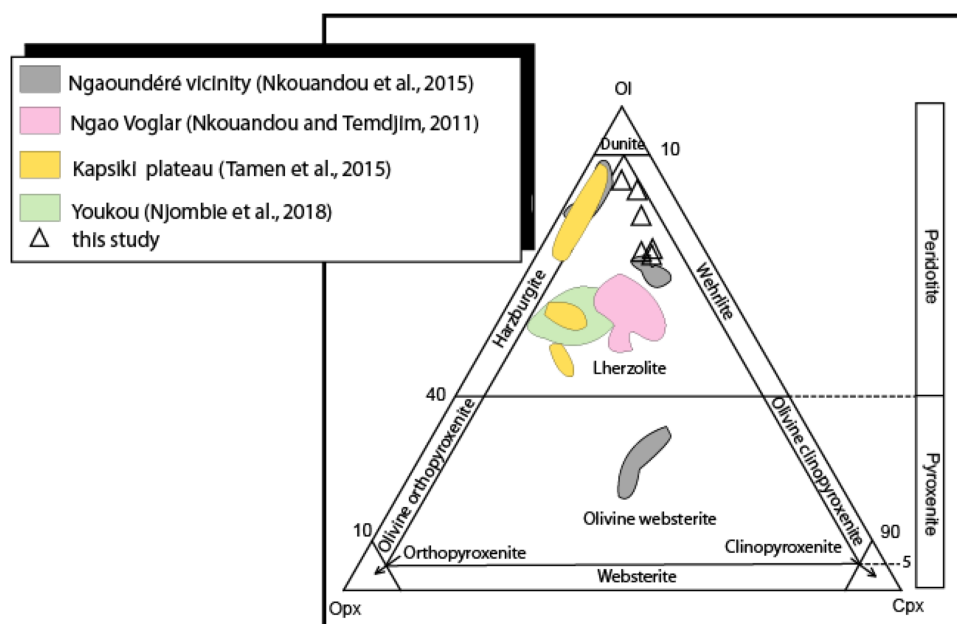


Fig. 3 Photomicrographs of thin sections showing textural variations of basaltic host lava (**A**) and studied xenoliths (**B** to **F**). **A** Microlitic porphyritic texture of basaltic host lava, **B** Protoplanular texture showing triple point junction between olivine crystals, **C** Interstitial spinel crystals showing reaction zones, **D** Iddingsitisation of olivine crystals evidencing fluid infiltration, **E** Sharp contact between pyroxene and olivine and host lava, **F** Contact between host lava and skeletal aspect of studied xenolith. *ox*/oxide, *sp*/spinel

Table 2 Modal compositions of Hosséré Séde xenoliths

Sample	Olivine	Clinopyroxene	Orthopyroxene	Spinel
A36	76	14	8	2
A38	67	18	12	3
S28	69	20	10	1
A35	67	17	11	5
S20	81	11	6	2
F12	84	7	8	1

Fig. 4 Modal compositions of peridotite xenoliths from Hosséré Séde volcano



altitude of 1365 m (Fig. 2A) and towering 144 m above the basement, was emplaced at the crossing of the 70°N and 135°N Pan African fault network of the northern Ngaoundéré area as fissural volcanism. Hosséré Séde volcano forms a dome shape form without a crater, 280 m in diameter, with gentle slopes. The volume of basaltic lavas is 11 500 000 m³. Hosséré Séde volcano does not display lava flows but 25–70 cm basaltic blocks and rare up to 1.7 m boulders, with 5–10 cm cavities (Fig. 2B). Some of them contain fragments of mantle peridotite (Fig. 2C). The top of Hosséré volcano is essentially covered by small (< 40 cm in size) blocks, whereas, at the base, larger (0.7–1.7 m) blocks hide the contact with the granitoid basement.

Basaltic blocks, coated by thin 2–5 mm brown patina, are composed of a dark matrix containing phenocrysts of olivine (3–6 mm, 10–15 vol%), pyroxene (2–5 mm, 5–8 vol%) and sparkling microliths of plagioclase (25–30 vol %). Under the microscope (Fig. 3A), basalt shows porphyritic microlitic texture. Olivine xenocrysts are free of oxide inclusions, contrary to olivine phenocrysts including oxide microcrystals. Minute plagioclase microliths are frequently associated with oxide microcrystals.

We observe numerous xenoliths transported to the surface by the basalt. These are more or less altered peridotite enclaves or crumbly granitoid xenoliths. Contacts between xenoliths and basaltic host lava are sharp.

Angular peridotite xenoliths are 6–12 cm long (Fig. 2C). They are mainly composed of four minerals—olivine, clinopyroxene, orthopyroxene, and spinel (Fig. 3). Large yellow-greenish olivine crystals (67–84 vol%, Table 2) strongly predominate, clinopyroxene crystals are 7–20 vol %, orthopyroxene represent 6–12 % and spinel are 1–5 vol

%. No hydrous phases, such as amphibole or phlogopite, were observed. The studied xenoliths are classified as spinel Iherzolite (Fig. 4) as proposed by Le Maître (2002).

On plate polarised light, all xenoliths exhibit typical protogranular texture, except sample A12 which exhibits equigranular texture after the classification scheme of Mercier and Nicolas (1975). Olivine grains have sizes ranging from 2 to 5 mm, orthopyroxene, and clinopyroxene are 1.5–3.5 mm in size, while spinel is generally 1–2 mm. Spinel occurs as discrete, dispersed, or interstitial grains frequently between olivine and orthopyroxene (Fig. 3C). Thin reaction zones always develop around spinel crystals that resemble spongy rims (Fig. 3C). In most samples of equigranular texture, olivine phases show iddingsitized boundaries expressed as thin (20–50 µm) yellowish bands (Fig. 3D). Contacts between xenoliths and host basaltic lava are sharp (Fig. 3E), but sometimes develop skeletal structure (Fig. 3F).

4.2 Mineralogy

4.2.1 Host lava

Chemical analyses of the main mineral phases of the host basaltic lava are listed in Table 3.

Olivine phenocryst cores have higher Fo (=100 Mg / Mg + Fe) (Fo₈₁) than rims (Fo₇₆₋₇₇) and microcrysts (Fo₇₀₋₇₄). CaO contents vary from 0.11 wt% in phenocryst cores to 0.46 wt% in microcrysts while NiO contents (0.13–0.21 wt%) remain relatively low.

Clinopyroxene phenocrysts are mainly diopside in composition (Wo_{49.5-51} En₃₆₋₃₉ Fs₅₁₂₋₁₃) after the

Table 3 Chemical compositions and structural formulas of main minerals of host basaltic lava

Sample Mineral Description No.	A36 olivine mic	S20 ph.c 3	A36 cpx 5	S20 ph.c 8	F12 pl 11	A36 pl 12	F12 pl 13	A36 pl 14	F12 pl 15	analcite	F12 Ti-int	S20 Ti-int
SiO ₂ (wt %)	38.67	38.12	35.76	40.08	38.28	44.70	47.22	44.21	45.50	45.95	44.91	59.37
TiO ₂					3.94	2.80	4.48	3.55	3.40	3.65		
Al ₂ O ₃					8.07	5.26	8.62	7.27	7.00	7.67	24.12	25.07
Cr ₂ O ₃					0.02	0.03	0.04	0.06	0.04	0.00	26.39	24.35
FeOt	21.27	23.11	26.75	17.81	21.00	7.39	7.16	7.25	6.85	6.68	7.35	0.37
MnO	0.50	0.54	0.61	0.25	0.41	0.13	0.17	0.15	0.21	0.11	0.11	1.39
MgO	38.40	37.64	35.70	43.41	39.52	11.73	13.27	11.43	12.49	12.66	12.04	0.41
CaO	0.35	0.46	0.43	0.11	0.43	22.45	22.65	22.51	22.42	22.56	22.49	0.31
NiO	0.18	0.13	0.19	0.21	0.18	0.00	0.02	0.00	0.02	0.01	0.01	1.25
Na ₂ O					0.59	0.61	0.65	0.68	0.62	0.69	6.89	7.85
K ₂ O											6.31	15.39
BaO											3.12	1.38
sum	99.37	100.00	99.44	101.87	99.82	99.02	99.19	99.34	99.03	99.04	98.92	99.06
Si (apfu)	1.009	0.998	0.965	1.000	0.994	6.737	7.066	6.650	6.826	6.889	6.758	2.702
Ti					0.447	0.315	0.507	0.401	0.383	0.413	2.640	2.579
Al					1.433	0.928	1.528	1.286	1.236	1.361	1.294	1.354
Cr					0.002	0.004	0.005	0.007	0.005	0.000	1.413	1.317
Fe ³⁺					0.370	0.484	0.344	0.452	0.395	0.498		
Fe ²⁺	0.464	0.506	0.604	0.372	0.456	0.562	0.412	0.568	0.408	0.443	0.427	0.000
Mn	0.011	0.012	0.014	0.005	0.009	0.017	0.022	0.019	0.027	0.014	0.014	0.000
Mg	1.493	1.469	1.436	1.615	1.530	2.635	2.595	2.562	2.793	2.828	2.700	0.000
Ca	0.010	0.013	0.012	0.003	0.012	3.625	3.632	3.628	3.604	3.624	3.626	0.251
Ni	0.004	0.003	0.004	0.004	0.004	0.000	0.002	0.000	0.000	0.002	0.001	0.015
Na	0.001	0.001	0.001	0.001	0.001	0.172	0.177	0.190	0.198	0.180	0.201	0.608
K											0.563	1.362
Ba											0.568	1.195
Fe ₂ O ₃ *					3.26	4.30	3.04	4.00	3.50	4.40		
FeO*					4.46	3.29	4.52	3.25	3.53	3.39		
Wo					50.30	48.37	50.94	49.49	49.62	49.91		
En					36.55	39.41	35.98	38.34	38.73	37.16		
Fs					13.15	12.22	13.08	12.17	11.66	12.92		
Fo	75.87	73.93	69.93	81.08	76.69							18.06
Fa	24.13	26.07	30.07	18.92	23.31							46.79

Table 3 continued

Sample	A36	S20		A36	S20	F12	A36												
Mineral	olivine			cpx			pl												
Description	mic		ph.c	mic	ph.c	ml		ph.c											
No.	1	2	3	4	5	6		9	10	11	12	13	14	15	16	17	18	19	20
Or									12.34	7.77	5.70	13.69							
Ab									62.06	57.64	56.38	56.75							
An									25.60	34.59	37.92	29.75							
Ulvöspinel																			66.57

Oxide structural formula calculated after Carmichael (1967); olivine on the basis of 4 oxygen anions, clinopyroxene on the basis of 16 cations, plagioclase and “feldspathoid” on the basis of 8 oxygen anions, Ti-magnetite on the basis of 4 oxygen anions
ph phenocryst, *c* core, *m*/microlith, *mic* microcryst, *mt*/magnetite

classification scheme of Morimoto et al. (1988) with minor microliths of less calcic composition (Wo_{48} En_{39} Fs_{12}). TiO_2 (2.80–4.48 wt%) and Al_2O_3 (5.26–8.62 wt%) contents of clinopyroxene are relatively high. Na_2O contents (0.59–0.69 wt%) are relatively constant. Note that the clinopyroxene phenocrysts with $\text{Wo} > 50$ wt% witness fassaitic compositions like in alkali basalts described by Wandji et al. (2000) in Noun Plain, Cameroon.

Plagioclase crystals (An_{38-26} Ab_{56-62} Or_{6-14}) are mostly andesine to oligoclase.

Moreover, some mineral phases, Na_2O (10.3–15.9 wt%) and K_2O (1.6–6.8 wt%) rich, present affinities with analcite that give a basanitic character to the host lava.

Ti-oxide is titanomagnetite—titanohematite (TiO_2 : 22.71 wt%; Fe_2O_3 : 18.06 wt% and FeO : 46.79 wt%) with 66.57% ulvöspinel.

4.2.2 Peridotite xenoliths

Chemical compositions of olivine, clinopyroxene, orthopyroxene, and spinel are listed in Tables 4, 5, 6, 7.

Olivine crystals are highly magnesian (Fo_{88-90}) (Table 4). Low CaO contents (<0.1 wt%) are typical of mantle olivine, except in olivine rims in contact with basaltic host lavas (0.11–0.27 wt%) (Fig. 5). NiO contents are high (up to 0.42 wt%) compared to olivine crystals of host basaltic lava (Table 3, Fig. 6).

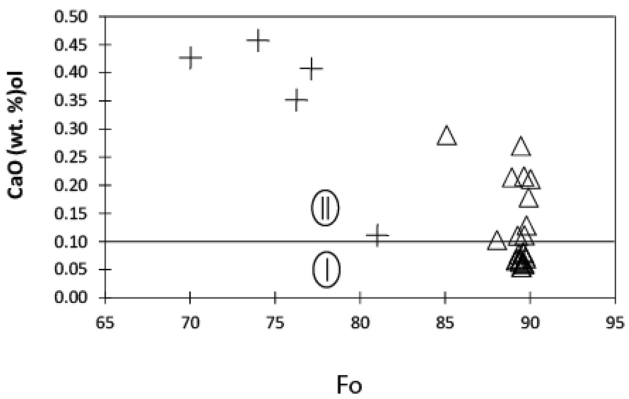
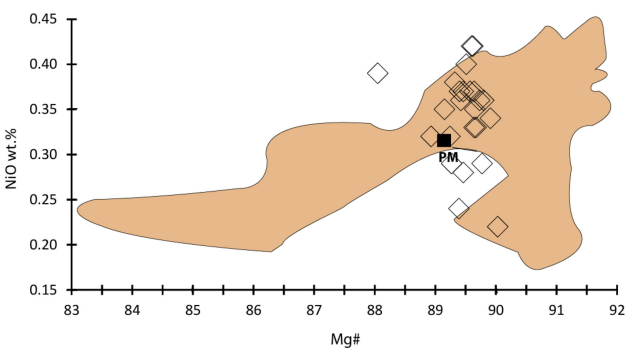
Clinopyroxene is diopside and augite (Wo_{42-50} En_{45-54} Fs_{4-6}) (Table 5, Fig. 7) after Morimoto et al. (1988). Mg# ratios (=100 $\text{Mg} / (\text{Mg} + \text{Fe})$) are high (88.8–92.5) for both diopside and augite, typical of mantle clinopyroxene (Fig. 8). TiO_2 contents are low (0.20–1.53 wt%). Al_2O_3 contents vary widely (0.64–10.61 wt%) whereas Cr_2O_3 contents (0.74–1.34 wt%) are rather high, defining typical Al-Cr clinopyroxenes after Morimoto et al. (1988). Two groups of clinopyroxenes are evidenced: (i) one group (4 analyses) is Al_2O_3 (6.8–10.6 wt%) and Na_2O (1.2–1.9 wt %) rich, which include jadeite molecule and (ii) another group (12 analyses), Al_2O_3 (0.6–4.8 wt%) and Na_2O (0.4–0.6 wt%) poorer.

Orthopyroxene is enstatite ($\text{Wo}_{1.5}$ En_{89} $\text{Fs}_{9.5}$) type (Table 6, Fig. 7) after Morimoto et al. (1988). Mg# ratios are high (90.1–90.5), typical of mantle orthopyroxene (Fig. 9). TiO_2 contents (0.10–0.13 wt%) are very low. Al_2O_3 contents are constant (4.55–4.61 wt%). Na_2O contents are also low (0.10–0.15 wt%).

Spinel is dominantly Al-spinel (Al_2O_3 up to 56 wt%) after Carswell (1980) (Table 7). Few crystals are Cr-spinels, with high Cr_2O_3 contents (49.15 wt%). FeO contents in Al-type are lower (11.33–13.79 wt%) than in Cr-type (21.62 wt%). MgO contents are higher (19.52–20.79 wt%) in Al-spinel than in Cr-spinel (10.05 wt%). Al-spinel has higher NiO contents (0.30–0.45 wt%) than Cr-spinel (0.08

Table 4 Olivine compositions of Hossére Sédé xenoliths and structural formulas on the basis of 4 oxygen anions

Sample No.	A36						S20						F12											
	1	2	3	4	5	6	7	8	9	10	11	12	13	14	15	16	17	18	19	20	21	22	23	24
SiO ₂	41.02	41.10	40.85	40.32	41.00	40.65	40.73	41.08	42.07	41.26	41.05	41.16	41.45	40.49	41.07	41.06	41.02	40.90	40.79	41.47	41.07	41.49	41.17	40.11
FeO	9.94	11.07	10.12	10.43	10.30	9.83	9.86	10.25	9.91	10.02	10.11	9.95	9.91	9.81	9.71	10.14	10.21	10.30	9.95	9.97	10.09	9.93	10.05	9.69
MnO	0.15	0.12	0.13	0.17	0.14	0.15	0.07	0.15	0.10	0.13	0.19	0.26	0.17	0.22	0.18	0.20	0.14	0.14	0.17	0.13	0.09	0.09	0.13	0.14
MgO	47.86	46.31	47.69	47.72	48.15	48.49	48.84	48.53	48.37	48.59	48.70	48.59	48.96	49.53	49.49	49.23	48.88	48.99	48.78	49.19	49.32	49.08	49.42	49.79
CaO	0.07	0.10	0.07	0.21	0.07	0.06	0.07	0.11	0.08	0.05	0.06	0.27	0.22	0.13	0.18	0.05	0.07	0.08	0.06	0.11	0.08	0.07	0.06	0.21
NiO	0.36	0.39	0.32	0.32	0.35	0.35	0.29	0.29	0.42	0.40	0.37	0.28	0.33	0.36	0.34	0.37	0.24	0.38	0.37	0.33	0.42	0.36	0.37	0.22
sum	99.40	99.09	99.18	99.17	100.01	99.53	99.86	100.41	100.95	100.45	100.48	100.51	101.04	100.54	100.97	101.05	100.56	100.79	100.12	101.20	101.07	101.02	101.20	100.16
Si (apfu)	1.011	1.021	1.010	1.001	1.007	1.002	1.000	1.005	1.019	1.007	1.003	1.005	1.006	0.990	0.998	1.001	0.998	1.000	1.005	0.998	1.000	0.999	0.984	
Fe ²⁺	0.205	0.230	0.209	0.216	0.212	0.203	0.202	0.210	0.201	0.204	0.206	0.203	0.201	0.201	0.197	0.206	0.208	0.210	0.204	0.202	0.205	0.201	0.204	0.199
Mn	0.003	0.003	0.003	0.004	0.003	0.003	0.001	0.003	0.002	0.003	0.004	0.005	0.004	0.004	0.004	0.004	0.003	0.003	0.004	0.003	0.002	0.002	0.003	0.003
Mg	1.760	1.715	1.758	1.766	1.763	1.782	1.788	1.769	1.748	1.768	1.774	1.769	1.771	1.805	1.792	1.784	1.779	1.782	1.783	1.776	1.787	1.775	1.787	1.821
Ca	0.002	0.003	0.002	0.006	0.002	0.002	0.002	0.002	0.003	0.001	0.002	0.007	0.006	0.003	0.005	0.001	0.001	0.002	0.002	0.003	0.002	0.002	0.002	0.006
Ni	0.007	0.008	0.006	0.006	0.007	0.007	0.006	0.006	0.008	0.008	0.007	0.005	0.006	0.007	0.007	0.007	0.005	0.008	0.007	0.007	0.007	0.007	0.004	
Fo	89.42	88.05	89.24	88.93	89.15	89.65	89.77	89.27	89.60	89.51	89.40	89.46	89.64	89.80	89.91	89.46	89.39	89.32	89.57	89.67	89.73	89.64	89.03	

**Fig. 5** CaO vs Fo diagram for olivine from Hossére Sédé. Field I for olivine mantle peridotites and field II for magmatic olivine after Simkin and Smith (1970). Cross=host lava, open triangle=lherzolite**Fig. 6** NiO vs Mg# (Fo) diagram for olivine from Hossére Sédé. In brown, field of “West Eifel and Siebengebirge ultramafic xenoliths” after Rizzo et al (2021)

wt%). Cr# of Cr-spinel is 73.76 and lower in Al-spinel (11.68–17.63). Mg# is higher in Al-spinel crystals (77.08–80.34) than in Cr-spinel (48.06). Fe³⁺# [=100*Fe³⁺ / (Fe³⁺ + Al³⁺ + Cr³⁺)] ratios of Al-spinel range between 2.16 and 4.31 while those of Cr-spinel (3.44) overlap Al-spinel values. Cr-spinel shares affinities with some Cr-spinels (Cr₂O₃=46.2–49.5 wt%, Al₂O₃=16.2–19.5 wt%, MgO=13.1–13.5 wt%, FeO^t (total)=19.22–19.57 wt%, NiO=0.14–0.16 wt%) that exist in xenoliths from Scotland (Upton et al. 2011). Reversely, Cr-spinel described in Mt. Vulture, Italy (Cr₂O₃=40.2 wt%, Al₂O₃=25.0 wt%, MgO=15.7 wt%, FeO^t=22.1 wt%, NiO=0.2 wt%; Jones et al. 2000) is Cr-poorer but Al-richer. By comparison, Cr-spinel of Andaman ophiolite (Ghosh et al. 2012, 2013) is far Cr-richer (Cr₂O₃=55 wt%, Al₂O₃=15 wt%, MgO=14 wt%, FeO^t=17 wt%, NiO=0.1 wt%). Rizzo et al. (2021) described spinels with Cr# between 9.5 and 57.2 in West Eifel ultramafic xenoliths.

Table 5 Clinopyroxene compositions of Hosséié Sédé xenoliths and structural formulas on the basis of 16 cations and 24 oxygen anions

Sample No.	A36	1	2	3	4	5	6	7	8	9	10	11	12	13	14	15	16	17
SiO ₂ (wt %)	51.19	52.10	54.04	52.10	51.71	50.48	55.06	54.46	51.45	52.29	51.84	52.14	54.72	52.25	51.86	52.40	52.27	
TiO ₂	0.72	0.69	0.71	0.69	0.72	1.35	0.20	0.28	0.39	0.53	0.47	0.44	0.29	1.53	0.43	0.90	0.43	
Al ₂ O ₃	3.89	3.19	10.61	3.98	3.25	4.32	0.87	0.89	6.82	3.25	4.79	6.92	0.64	2.55	7.37	1.86	7.06	
Cr ₂ O ₃	1.00	1.34	0.77	0.81	1.02	1.06	0.74	1.08	0.83	0.86	0.83	0.78	0.93	1.13	0.84	0.85	0.85	
FeOt	3.25	2.81	2.36	3.52	3.20	3.44	2.80	2.71	3.07	3.71	3.15	3.19	2.90	2.55	3.00	3.21	3.00	
MnO	0.08	0.07	0.04	0.07	0.08	0.06	0.13	0.09	0.09	0.09	0.08	0.08	0.09	0.05	0.07	0.11	0.09	
MgO	16.02	16.63	12.11	16.43	16.20	15.35	19.00	18.67	14.99	17.58	16.46	15.39	19.24	17.03	15.95	17.04	15.10	
NiO	0.00	0.00	0.00	0.07	0.12	0.00	0.11	0.04	0.05	0.00	0.09	0.12	0.00	0.00	0.03	0.00	0.00	
CaO	22.53	23.02	18.40	22.37	23.08	23.00	21.05	21.21	19.16	20.75	21.99	19.46	20.71	22.22	19.70	21.90	19.47	
Na ₂ O	0.52	0.59	1.82	0.52	0.53	0.54	0.48	0.47	1.94	0.57	0.44	1.62	0.49	0.59	1.16	0.45	2.04	
sum	99.20	100.44	100.86	100.56	99.91	99.60	100.44	99.90	98.79	99.63	100.14	100.14	100.01	99.90	100.41	98.72	100.31	
Si (apfu)	7.520	7.548	7.790	7.546	7.547	7.415	7.925	7.892	7.500	7.612	7.526	7.515	7.906	7.613	7.458	7.731	7.501	
Ti	0.080	0.075	0.077	0.075	0.079	0.149	0.022	0.031	0.043	0.058	0.051	0.048	0.032	0.168	0.047	0.100	0.046	
Al ^{IV}	0.480	0.452	0.210	0.454	0.453	0.585	0.075	0.108	0.500	0.388	0.474	0.485	0.094	0.387	0.542	0.269	0.499	
Al ^{VI}	0.193	0.093	1.593	0.225	0.106	0.163	0.073	0.044	0.672	0.169	0.345	0.691	0.015	0.051	0.708	0.054	0.695	
Cr	0.116	0.153	0.088	0.093	0.118	0.123	0.084	0.124	0.096	0.099	0.095	0.089	0.106	0.130	0.095	0.099	0.096	
Fe ³⁺	0.160	0.221	0.000	0.132	0.222	0.154	0.009	0.011	0.194	0.165	0.055	0.062	0.047	0.037	0.000	0.045	0.182	
Fe ²⁺	0.240	0.119	0.285	0.294	0.169	0.269	0.328	0.317	0.180	0.287	0.327	0.322	0.303	0.274	0.361	0.351	0.178	
Mn	0.010	0.009	0.005	0.009	0.010	0.007	0.016	0.011	0.011	0.011	0.010	0.010	0.011	0.006	0.009	0.014	0.011	
Mg	3.507	3.591	2.602	3.546	3.524	3.360	4.076	4.032	3.257	3.814	3.561	3.306	4.143	3.698	3.419	3.747	3.229	
Ni	0.000	0.000	0.000	0.008	0.014	0.000	0.013	0.005	0.006	0.000	0.011	0.014	0.000	0.000	0.003	0.000	0.000	
Ca	3.546	3.573	2.842	3.472	3.609	3.620	3.246	3.293	2.993	3.236	3.421	3.006	3.206	3.469	3.036	3.462	2.994	
Na	0.148	0.166	0.509	0.146	0.150	0.154	0.134	0.132	0.548	0.161	0.124	0.453	0.137	0.167	0.323	0.129	0.568	
FeO*	1.95	0.98	2.36	2.43	1.38	2.19	2.73	2.62	1.48	2.35	2.69	2.67	2.51	2.25	3.00	2.84	1.48	
Fe ₂ O ₃ *	1.44	2.03	0.00	1.21	2.02	1.39	0.08	0.10	1.77	1.51	0.51	0.57	0.44	0.33	0.00	0.41	1.69	
Mg/Mg+Fe ^t	89.78	91.34	90.14	89.27	90.02	88.83	92.36	92.47	89.69	89.41	90.30	89.58	92.20	90.45	90.44	89.97		
Wo	47.52	49.57	46.58	47.91	48.85	42.30	42.97	45.11	43.08	46.39	44.82	41.58	46.35	44.49	45.44	45.40		
En	47.00	47.79	45.38	46.77	45.35	53.10	52.60	49.08	50.76	48.29	49.30	53.73	49.41	50.10	49.18	48.97		
Fs	5.48	4.65	5.05	5.84	5.32	5.80	4.60	4.43	5.81	6.16	5.32	5.88	4.69	4.23	5.41	5.38	5.63	

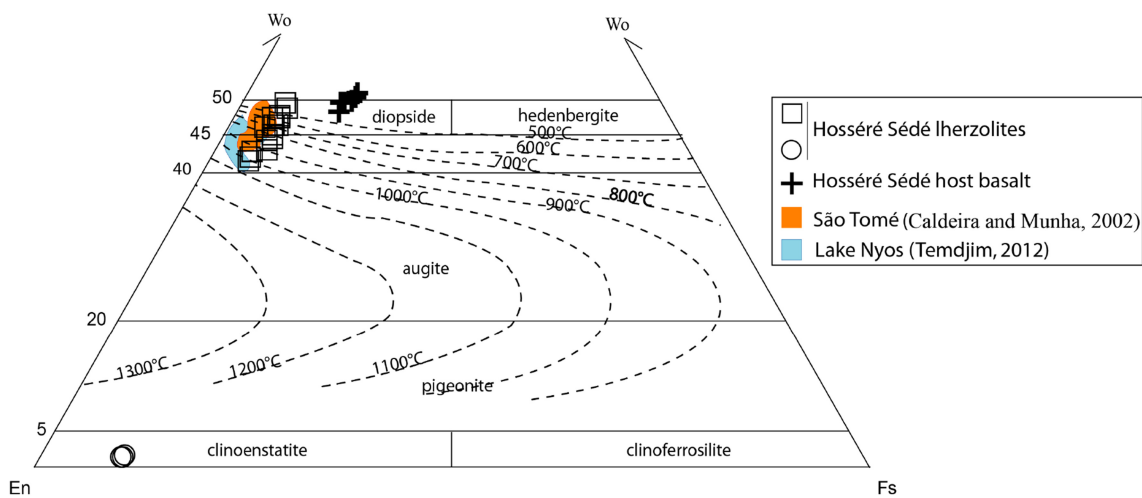


Fig. 7 Pyroxene chemical compositions of host lava and lherzolite xenoliths from Hossére Sédé volcano in quadrilateral diagram after Morimoto et al. (1988). Clinopyroxenes of peridotites of Lake Nyos, Cameroon, and São Tomé Island are plotted for comparison. Thermometric curves between 500 and 1300 °C according to Lindsley (1983) for P=5 kbar (0.5 GPa). Open square=clinopyroxene, open circle=orthopyroxene

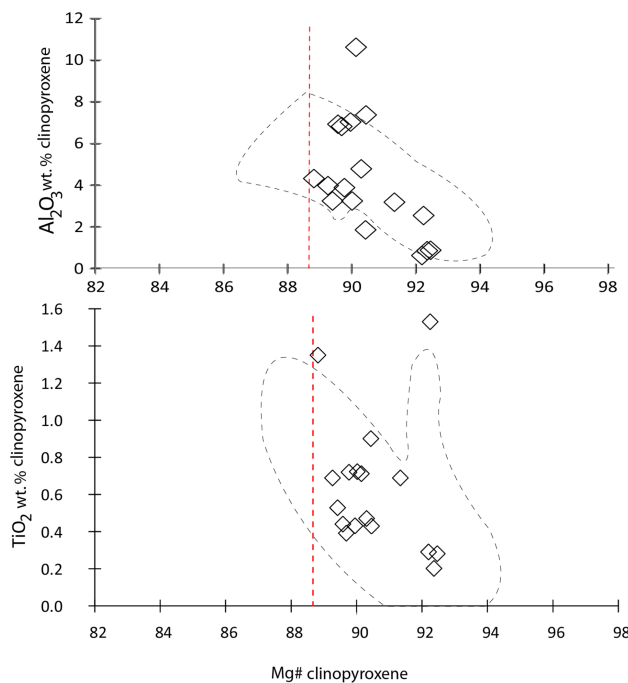


Fig. 8 **A** Al_2O_3 vs. Mg# and **B** TiO_2 vs. Mg# of clinopyroxene of peridotite xenoliths. Dashed line=field of “West Eifel and Siebengebirge ultramafic xenoliths” after Rizzo et al (2021). Dashed vertical lines represent the Mg# thresholds used to discriminate between cumulates and mantle clinopyroxene

On Cr# vs Fo OSMA diagram (Fig. 10, Arai 1994), studied xenoliths plot in mantle array, except one relative to the Cr-spinel.

4.2.3 Thermobarometry

Graphical estimation with curves defined by Lindsley (1983) in En-Wo-Fs quadrilateral scheme of clinopyroxene (Fig. 7) gives a wide range of temperatures, with a maximum value of about 1020 °C, for a pressure of 5 kbars (0.5 GPa) but note that these thermometric curves are nearly the same between 1 atm and 10 kbar (1 GPa).

The results of the equilibrium temperature estimated for several pyroxene crystals of sample A36, through empirical thermometers, are listed in Table 8. O’Neill and Wall (1987) method gives a temperature range of 902–1045 °C, assuming a mantle pressure of 15 kbar (1.5 GPa) following these two authors. Temperature calculations after Mercier (1980) using Cr-Al solubility in clinopyroxene give similar equilibrium temperatures between 852 and 1028 °C with also three other higher values (1108–1204 °C). Wells (1977) formula based on clinopyroxene/orthopyroxene Ca-exchange yields a temperature range of 914–1105±50 °C. Putirka (2008) two pyroxenes geothermometer give both low values (936–1018 °C) and higher values between 1086

Table 6 Orthopyroxene compositions of Hossére Sédé xenoliths and structural formulas on the basis of 16 cations and 24 oxygen anions

Sample No	A36 1	2	F12 3
SiO ₂ (wt %)	54.78	55.01	55.21
TiO ₂	0.12	0.10	0.13
Al ₂ O ₃	4.61	4.56	4.55
Cr ₂ O ₃	0.38	0.45	0.34
FeOt	6.33	6.37	6.23
MnO	0.17	0.08	0.15
MgO	32.59	32.83	33.18
NiO	0.18	0.14	0.07
CaO	0.78	0.71	0.74
Na ₂ O	0.15	0.10	0.14
sum	100.09	100.35	100.74
Si (apfu)	7.563	7.574	7.560
Ti	0.012	0.010	0.013
Al ^{IV}	0.437	0.426	0.440
Al ^{VI}	0.314	0.314	0.294
Cr	0.041	0.049	0.037
Fe ³⁺	0.097	0.069	0.119
Fe ²⁺	0.634	0.665	0.594
Mn	0.020	0.009	0.017
Mg	6.706	6.737	6.771
Ni	0.020	0.016	0.008
Ca	0.115	0.105	0.109
Na	0.040	0.027	0.037
FeO*	5.49	5.77	5.19
Fe ₂ O ₃ *	0.93	0.66	1.16
Mg/Mg+Fe ²⁺	90.17	90.18	90.47
Wo	1.52	1.38	1.43
En	88.56	88.82	88.97
Fs	9.92	9.79	9.60

and 1119 °C. Brey and Köhler (1990) two pyroxenes geothermometer give various values, high (1095–1164 °C) or lower (866–1070 °C). From these five geothermometers, the highest values (1085–1204 °C) seem to represent equilibria while lower ones (852–1070 °C) evidence late re-equilibration of the xenoliths (Nkouandou et al. 2015).

Calculated pressures using Mercier (1980) formulas give equilibrium pressures of 1.07–1.35 GPa, while Putirka (2008) barometer gives 1.08–1.57 GPa, except one value at 0.60 GPa. The corresponding depths are bracketed between

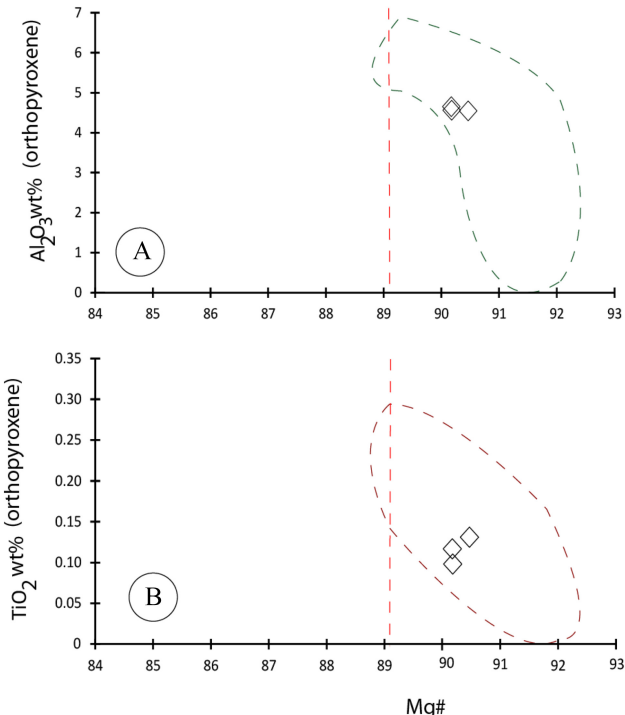


Fig. 9 **A** Al₂O₃ vs. Mg# and **B** TiO₂ vs. Mg# of orthopyroxene of peridotite xenoliths. Dashed line=field of “West Eifel and Siebengebirge ultramafic xenoliths” after Rizzo et al (2021). Dashed vertical lines represent the Mg# thresholds used to discriminate between cumulates and mantle orthopyroxene

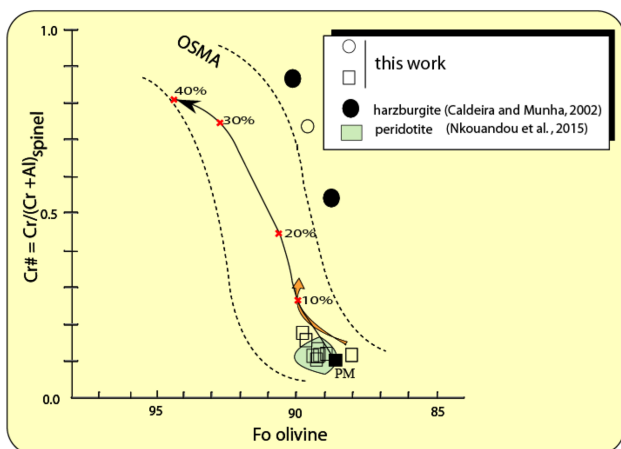
35.6 and 51.8 km when using the conversion factor of 33 km × GPa⁻¹, corresponding to the sampling depth (Fig. 11). The pressures calculated for Hossére Sédé xenoliths are in the 1.0 to 2.0 GPa range of those estimated by different authors (experimentations by O’Neill 1981; Gasparik 1987).

5 Discussion

Various petrological studies on mantle peridotites sampled by basaltic lavas on their way to the surface (Nkouandou and Temdjim 2011; Nkouandou et al. 2015; Njombie et al. 2018) reveal the complexity of composition and structure of lithospheric mantle under Adamawa plateau, which may have evolved through the melting process. Moreover, metasomatism by a carbonatitic fluid phase could have occurred as witnessed by possible spongy rims on spinel (Fig. 3C) (Carpenter et al. 2002).

Table 7 Spinel compositions of Hosséhé Sédé xenoliths and structural formulas on the basis of 32 oxygen anions

Mineral Sample No.	Al-spl A36 1	Al-spl A36 2	Al-spl A36 3	Al-spl A36 4	Al-spl A36 5	Al-spl A36 6	Cr-spl A36 7	Al-spl S20 8	Al-spl S20 9
TiO ₂	0.17	0.17	0.15	0.19	0.14	1.81	2.29	2.06	0.12
Al ₂ O ₃	55.63	55.46	55.10	53.06	55.89	48.56	11.73	47.47	55.95
Cr ₂ O ₃	10.97	11.19	11.00	11.18	11.54	13.61	49.15	15.15	11.08
FeO	11.64	12.03	11.55	13.79	11.33	12.74	21.62	13.77	11.52
MgO	20.62	20.50	20.71	19.52	20.79	19.92	10.05	19.76	20.49
CaO	0.00	0.01	0.01	0.01	0.00	0.06	0.12	0.01	0.00
NiO	0.40	0.31	0.40	0.41	0.41	0.45	0.08	0.36	0.30
sum	99.43	99.67	98.92	98.16	100.10	97.15	95.04	98.58	99.46
Ti (apfu)	0.026	0.027	0.023	0.030	0.022	0.297	0.470	0.336	0.018
Al	13.652	13.590	13.550	13.328	13.627	12.453	3.770	12.119	13.721
Cr	1.806	1.840	1.815	1.885	1.887	2.342	10.598	2.594	1.822
Fe ³⁺	0.449	0.430	0.427	0.685	0.391	0.538	0.512	0.597	0.363
Fe ²⁺	1.578	1.661	1.590	1.774	1.569	1.780	4.419	1.897	1.640
Mg	6.401	6.355	6.443	6.204	6.411	6.461	4.088	6.382	6.356
Ca	0.000	0.002	0.003	0.003	0.000	0.014	0.034	0.002	0.000
Ni	0.068	0.052	0.068	0.070	0.068	0.079	0.019	0.064	0.050
Cr/Al+Cr	11.68	11.92	11.82	12.39	12.16	15.83	73.76	17.63	11.72
Mg/Mg+Fe ²⁺	80.22	79.28	80.21	77.77	80.34	78.40	48.06	77.08	79.49

**Fig. 10** Cr# ($=\text{Cr}/(\text{Cr}+\text{Al})$) of spinel versus Fo of olivine crystals of Hosséhé Sédé xenoliths plotted in the Olivine Spinel Mantle Array (OSMA) diagram of Arai (1994). Primitive Mantle (PM) composition of olivine and spinel according to McDonough and Sun (1995) and Johnson et al. (1990). Black arrow refers to the melting model of Arai (1994) and numbers (10% to 40%) correspond to melt extracted percentages

Hosséhé Sédé lherzolite xenoliths display fertile mantle features: most olivine crystals are characterized by high Mg# ratios (88.05–90.03), high NiO (0.22–0.42 wt%) and low CaO (<0.1 wt%, see Simkin and Smith 1970) contents, except scarce crystals with fairly high CaO contents (0.13–

0.27 wt%), suggesting the probable involvement of other processes experienced by Adamawa lithospheric mantle. Compositional variations are noticed on mineral analyses: high (up to 10.61 wt%) or low (0.64–0.89 wt%) Al₂O₃ contents of clinopyroxene crystals, simultaneous occurrence of Al- and Cr-spinel crystals in the same sample, variations in TiO₂ contents (0.1–2.3 wt%) of spinels.

The most likely hypothesis which may explain these features is mantle upwelling under the studied area. The double distribution of clinopyroxene compositions (Mg-rich and Al-poor vs. Mg-poor and Al-rich, Fig. 12) as well as the double distribution of spinel (Cr# 65–90 vs. Cr# of 10–60), suggest different degrees of extracted melt (from 5%–10% until 20%–25%, Fig. 12) in the spinel stability field rather than two mantle stages with garnet peridotite and later spinel peridotite (see discussions in Rudnick et al. 1993; Melchiorre et al. 2020; Rizzo et al. 2021; Casetta et al. 2022). OSMA diagram (Fig. 10) argues for similar values of 5%–10% of extracted melt (for Al-spinel) until 25% for Cr-spinel.

In that way, previous geophysical data have emphasized a migration of lithosphere—asthenosphere boundary from 120 to 80 km under the whole Adamawa plateau (Browne and Fairhead 1983; Poudjom Djomani et al. 1992, 1997; Nnange et al. 2000) and abnormal hot mantle materials

Table 8 Estimated temperatures, pressures and sampling depths of Hosséré Sédé xenoliths

Sample/method	TOW Opx/Cpx (°C) (n0opx-n0cpx)	TM Cpx (°C) (n0cpx)	TW Opx/Cpx (°C) (n0opx-n0cpx)	TP Cpx/Opx (°C) (n0cpx-n0opx)	TBK Cpx/Opx (°C) (n0cpx-n0opx)
A36	902.28 (1–1)	920.71 (1)	932 (1–1)	1018.1 (3–2)	867.01 (1–1)
A36	930.59 (1–5)	876.07 (2)	914 (1–2)	936.8 (6–2)	1163.73 (3–3)
A36	915.71 (2–5)	875.12 (3)	988 (1–3)	1119.4 (13–2)	1160.27 (3–1)
A36	1045.11 (2–7)	852.52 (4)	974 (1–4)	1085.9 (15–2)	935.88 (4–3)
A36		1204.29 (5)	970 (2–4)		959.57 (16–3)
A36		1168.92 (6)	1105 (2–7)		1056.72 (8–1)
A36		1028.52 (7)	1088 (2–8)		928.50 (14–3)
A36		1108.22 (8)	1007 (1–11)		1070.48 (10–1)
A36		1020.61 (9)			865.62 (1–2)
A36		1013.91 (12)			1160.62 (3–2)
					1094.99 (13–1)
		PM Cpx (GPa)		PP Cpx/Opx (Gpa)	
A36		1.07 (1)		1.57 (3–2)	
A36		1.35 (7)		0.60 (6–2)	
A36		1.33 (12)		1.08 (13–2)	
A36				1.28 (15–2)	
		Depth M (km)		Depth P (km)	
A36		43.9 (1)		51.8 (3–2)	
A36		35.4 (7)		19.8 (6–2)	
A36		44.6 (12)		35.6 (13–2)	
A36				42.2 (15–2)	

TOW Opx/Cpx: Temperature calculation after O'Neill and Wall (1987) formula, using Opx/Cpx data. TM Cpx: Temperature calculation after Mercier (1980), using clinopyroxene data. TW Opx/Cpx: Temperature calculation after Wells (1977), using Opx/Cpx data. TP Cpx/Opx: Temperature calculation after Putirka (2008) using Cpx/Opx equilibria; Temperature calculation after Brey and Köhler (1990) using Cpx/Opx equilibria. PM Cpx: Pressure calculation after Mercier (1980) formula, using clinopyroxene data. PP Cpx/Opx: Pressure calculation after Putirka (2008) using Cpx/Opx equilibria. GPa: gigapascal

located at depths between 70 and 90 km (Dorbath et al. 1986) coupled to adiabatic decompression.

Silica-undersaturated characteristics of Adamawa volcanism (Nkouandou et al. 2008, 2010, 2015) argue for mantle decompression related to crustal extension, indicating eroded sub-lithospheric mantle after upwelling (Hidas et al. 2019). The Hosséré Sédé mantle xenoliths may thus originate from evolution of spinel-bearing sub-continental lithospheric mantle controlled by mantle upwelling. Metasomatism process through melt infiltration could be also associated to this evolution so as tectonic work or re-work of Pan African strike slip faults delimiting the northern Adamawa plateau. Anyway, ongoing major and trace elements geochemical and Sr–Nd isotopic analyses on Hosséré Sédé lherzolites are mandatory to decipher the complex evolution underwent by the lithospheric mantle under the volcano.

6 Conclusion

Petrographical and detailed mineralogical studies carry out on Hosséré Sédé lherzolites in northern Ngaoundéré area evidence the complex history undergone by sub-lithospheric mantle under the Adamawa plateau.

Mineral phases in Hosséré Sédé lherzolites present larger ranges of chemical composition in comparison with some other lherzolites described in the Adamawa plateau (Nkouandou and Temdjim 2011; Nkouandou et al. 2015; Njombie et al. 2018). In that way, in Hosséré Sédé we note more various CaO contents in olivine, the occurrence of two groups of clinopyroxene, and the coexistence of two types of spinel.

The subcontinental mantle under the Adamawa plateau suffered partial melting extraction after decompression due

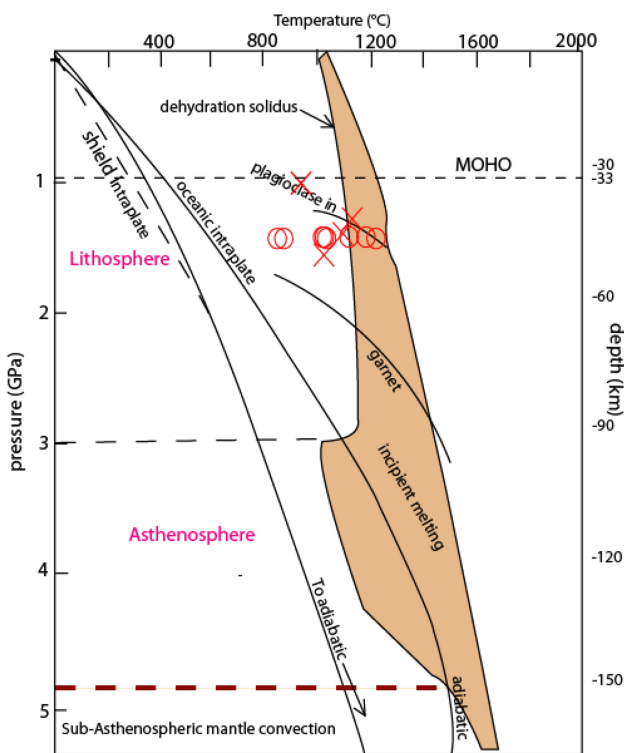


Fig. 11 Pressure–temperature–depth diagram for Hossére Sédé xenoliths (modified and adapted from Green and Falloon 1998)

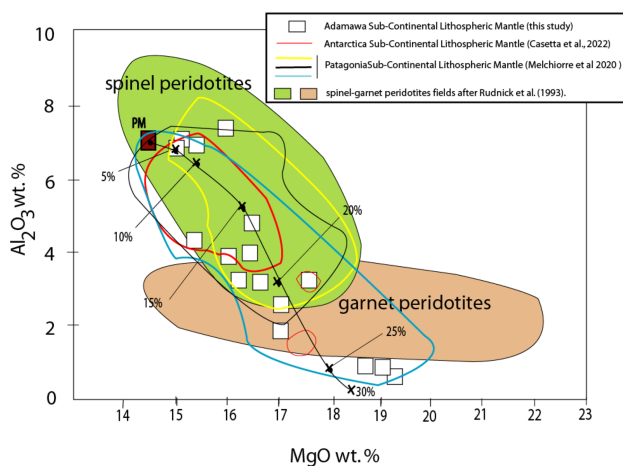


Fig. 12 Al_2O_3 versus MgO of clinopyroxene of Hossére Sédé xenoliths. Note that the analysis with $\text{Al}_2\text{O}_3 = 10.61 \text{ wt\%}$ and $\text{MgO} = 12.11 \text{ wt\%}$ plots outside of this diagram. Fields of the spinel peridotites and garnet peridotites after Rudnick et al. (1993). Fields of clinopyroxenes from Patagonia (Melchiorre et al. 2020) and from Antarctica (Casetta et al. 2022) added for comparison. Black curve indicates the melt extracted percentage, according to the melting model of Bonadiman and Coltorti (2011) and Upton et al. (2011), from a starting Primitive Mantle (PM) composition of Sun and McDonough (1989) and McDonough and Sun (1995)

to the migration of lithosphere–asthenosphere boundary. In addition, this mantle could have experienced metasomatism processes.

Acknowledgements Authors greatly thank the “Agence Universitaire de la Francophonie (AUF)” for financial support for microprobe analyses. We are grateful to the University of Paris-Saclay, France, for thin sections. Fruitful remarks by B. Bonin and A. Pouclet have greatly helped to improve the manuscript. F. Casetta and an anonymous reviewer are thanked for careful reviews.

Authors' contribution OFN, AFM, ZNN, AAS and HA made field studies, JMB made electron microprobe analyses, OFN and JMB prepared the manuscript.

Funding “Agence Universitaire de la Francophonie (AUF)”.

Data availability No.

Declarations Conflict of interest On behalf of all authors, the corresponding author states that there is no conflict of interest.

References

- Arai S (1994) Characterization of spinel peridotites by olivine–spinel compositional relationships: review and interpretation. *Chem Geol* 113(3–4):191–204
- Bonadiman C, Coltorti M (2011) Numerical modelling for peridotite phase melting trends in the $\text{SiO}_2\text{-Al}_2\text{O}_3\text{-FeO-MgO-CaO}$ system at 2 GPa. *Min Mag* 75:548
- Brey GP, Köhler T (1990) Geothermobarometry in four phase Iherzolites II. New thermobarometers, and practical assessment of existing thermometers. *J Petrol* 31:1353–1378
- Browne SE, Fairhead JD (1983) Gravity study of the Central African Rift System: a model of continental disruption 1. The Ngaoundéré and Abu Gabra rifts. In: Morgan P, Baker BH (eds). *Processes of planetary rifting*. *Tectonophysics* 94 (1–4), 187–203
- Caldeira R, Munhá JM (2002) Petrology of ultramafic nodules from São Tomé Island, Cameroon Volcanic Line (oceanic sector). *J Afr Earth Sc* 34(3–4):231–246
- Carmichael ISE (1967) The iron-titanium oxides of salic volcanic rocks and their associated ferromagnesian silicates. *Contrib Miner Petrol* 14(1):36–64
- Carpenter RL, Edgar AD, Thibault Y (2002) Origin of spongy textures in clinopyroxene and spinel from mantle xenoliths, Hessian Depression, Germany. *Min Petrol* 74:149–162
- Carswell DA (1980) Mantle derived Iherzolite nodules associated with kimberlite, carbonatite and basalt magmatism: a review. *Lithos* 13(2):121–138
- Casetta F, Rizzo AL, Faccini B, Ntaflos T, Abart R, Lanzafame G, Faccincani L, Mancini L, Giacomoni PP, Coltorti M (2022) CO_2 storage in the Antarctica sub-continental lithospheric mantle as revealed by intra- and inter-granular fluids. *Lithos* 416–417:106643
- Dorbath C, Dorbath L, Fairhead JD, Stuart GW (1986) A teleseismic delay time study across the Central African Shear Zone in the Adamawa region of Cameroon, West Africa. *Geophys J Int Royal Astron Soc* 86(3):751–766
- Dumont JF (1987) Étude structurale des bordures nord et sud du plateau de l’Adamaua: influence du contexte atlantique. *Géodynamique* 2(1):56–68
- Fagny AM, Nkouandou OF, Bardintzeff JM, Temdjam R, Guillou H (2016) Pétrologie du volcanisme Eocène-Oligocène du massif de

- Tchabal Mbabo, Adamaoua-Cameroun Afrique Centrale. Afrique Sci 12(6):35–47
- Fagny AM, Nkouandou OF, Bardintzeff JM, Guillou H, Iancu GO, Njankou Ndassa ZN, Temdjm R (2020) Petrology and geochemistry of the Tchabal Mbabo volcano in Cameroon volcanic line (Cameroon, Central Africa): an intra-continental alkaline volcanism. *J Afr Earth Sc* 170(103832):1–27
- Ganwa AA, Frisch W, Siebel W, Ekodeck GE, Cosmas SK, Ngako V (2008) Archean inheritances in the pyroxene-amphibole bearing gneiss of the Méiganga area (Central North Cameroon): geochemical and $^{207}\text{Pb}/^{206}\text{Pb}$ age imprints. *Comptes Rendus Géoscience* 340:211–222
- Gasparik T (1987) Orthopyroxene thermobarometry in simple and complex systems. *Contrib Min Petrol* 96:357–370
- Ghosh B, Morishita T, Bhatta K (2012) Detrital chromian spinels from beach placers of Andaman Islands, India: a perspective view of petrological characteristics and variations of the Andaman ophiolite. *Island Arc* 21:188–201
- Ghosh B, Morishita T, Bhatta K (2013) Significance of chromian spinels from the mantle sequence of the Andaman Ophiolite, India: Paleogeodynamic implications. *Lithos* 164–167:86–96
- Goussi Ngalamo JF, Basso D, Abdelsalam MG, Atekwana EA, Katumwehe AB, Ekodeck GE (2017) Geophysical imaging of metacratonization in the northern edge of the Congo craton in Cameroon. *J Afr Earth Sc* 129:94–107
- Green DH, Falloon TJ (1998) Pyrolite: A Ringwood concept and its current expression. In: Jackson I (ed) *The Earth's mantle: composition, structure, and evolution*. Cambridge University Press, Cambridge, pp 311–378
- Hidas K, Garrido CJ, Booth-Rea G, Marchesi C, Bodinier JL, Dautria JM, Louni-Hacini A, Azzouni-Sekkal A (2019) Lithosphere tearing along STEP faults and synkinematic formation of lherzolite and wehrlite in the shallow subcontinental mantle. *Solid Earth Discuss* 32:1–36
- Johnson KTM, Dick HJB, Shimizu N (1990) Melting in the oceanic upper mantle: an ion microprobe study of diopsides in abyssal peridotites. *J Geophys Res* 95:2661–2678
- Jones AP, Kostoula T, Stoppa F, Woolley AR (2000) Petrography and mineral chemistry of mantle xenoliths in a carbonate-rich melilititic tuff from Mt. Vulture volcano, Southern Italy. *Mineral Mag* 64(4):593–613
- Lindsley DH (1983) Pyroxene thermometry. *Am Min* 68(5–6):477–493
- Le Maitre RW (2002) Igneous rocks—A classification and glossary of terms. Recommendations of the IUGS Sub-Commission on the Systematics of Igneous Rocks, 2nd edition, Cambridge University Press, Cambridge, 252 p
- McDonough WF, Sun SS (1995) The composition of the Earth. *Chem Geol* 120(3–4):223–253
- Melchiorre M, Faccini B, Grégoire M, Benoit M, Casetta F, Coltorti M (2020) Melting and metasomatism/refertilisation processes in the Patagonian sub-continental lithospheric mantle: a review. *Lithos* 354–355:105324
- Mercier JCC (1980) Single-pyroxene thermobarometry. *Tectonophysics* 70:1–37
- Mercier JCC, Nicolas A (1975) Textures and fabrics of upper-mantle peridotites as illustrated by xenoliths from basalts. *J Petrol* 16 (2):454–487
- Moreau C, Regnault JM, Déruelle B, Bobineau B (1987) A new tectonic model for Cameroon line, central Africa. *Tectonophysics* 139:317–334
- Morimoto N, Fabriès J, Ferguson AK, Ginzburg IV, Ross M, Seifert FA, Zussman J, Aoki K, Gottardi G (1988) Nomenclature of pyroxenes. *Mineral Mag* 52:535–550
- Ngangom E (1983) Étude tectonique du fossé Crétacé de la Mbéré et du Djérem, Sud Adamawa, Cameroun. *Bull Centres De Recherches Exploration-Production, Elf-Aquitaine* 7:339–347
- Njankou Ndassa ZN, Nkouandou OF, Bardintzeff JM, Ganwa AA, Fagny Mefire A, Tizi A (2019) Petrology of peridotite host basaltic lavas of northern Ngaoundéré (Adamawa plateau, Cameroon, Central Africa). *Int J Adv Geosci* 7(2):85–94
- Njombie MPW, Temdjm R, Foley SF (2018) Petrology of spinel lherzolite xenoliths from Youkou volcano, Adamawa Massif, Cameroon Volcanic Line: mineralogical and geochemical fingerprints of sub-rift mantle processes. *Contrib Min Petrol* 173(13):1–21
- Nkouandou OF, Temdjm R (2011) Petrology of spinel lherzolite xenoliths and host basaltic lava from Ngao Voglar volcano, Adamawa Massif (Cameroon Volcanic Line, West Africa): equilibrium conditions and mantle characteristics. *J Geosci* 56:375–387
- Nkouandou OF, Ngounouno I, Déruelle B, Ohnenstetter D, Montigny R, Demaiffe D (2008) Petrology of the Mio-Pliocene Volcanism to the North and East of Ngaoundéré (Adamawa-Cameroun). *Comptes Rendus Géoscience* 340:27–38
- Nkouandou OF, Ngounouno I, Déruelle B (2010) Géochimie des laves basaltiques récentes des zones Nord et Est de Ngaoundéré (Plateau de l'Adamaoua, Cameroun, Afrique Centrale): pétrogenèse et nature de la source. *Int J Biol Chem Sci* 4(4):984–1003
- Nkouandou OF, Bardintzeff JM, Fagny AM (2015) Sub-continental lithospheric mantle structure beneath the Adamawa plateau inferred from the petrology of ultramafic xenoliths from Ngaoundéré (Adamawa plateau, Cameroon, Central Africa). *J Afr Earth Sc* 111:26–40
- Nnange JM, Ngako V, Fairhead JD, Ebinger CJ (2000) Depths to density discontinuities beneath the Adamawa Plateau region, Central Africa, from spectral analyses of new and existing gravity data. *J Afr Earth Sc* 30(4):887–901
- Nnange JM, Poudjom Djomani YH, Fairhead JD, Ebinger C (2001) Determination of the isostatic compensation mechanism of the region of the Adamawa dome, west central Africa using the admittance technique of gravity data. *Afr J Sci Technol (AJST), Sci Eng Series* 1(4):29–35
- O'Neill H, St C (1981) The transition between spinel lherzolite and garnet lherzolite, and its use as a geobarometer. *Contrib Miner Petrol* 77(2):185–194
- O'Neill H, St C, Wall VJ (1987) The olivine–orthopyroxene–spinel oxygen geobarometer, the nickel precipitation curve, and the oxygen fugacity of the Earth's upper mantle. *J Petrol* 28:1169–1191
- Ofoegbu CO (1984) A model for the tectonic evolution of the Benue Trough of Nigeria. *Geol Rundsch* 73(3):1007–1018
- Pouchou JL, Pichoir F (1991) Quantitative analysis of homogeneous or stratified microvolumes applying the model «PAP». In *Electron Probe quantification*; Heinrich DE; Newbury; Ed.; Plenum Press: New York, USA, 31–75
- Poudjom Djomani YH, Diament M, Albouy Y (1992) Mechanical behavior of the lithosphere Beneath the Adamawa Uplift (Cameroon, West Africa) based on gravity data. *J Afr Earth Sc* 15:81–90
- Poudjom Djomani YH, Nnange JM, Diament M, Ebinger CJ, Fairhead JD (1995) Effective elastic thickness and crustal thickness variation in west central Africa inferred from gravity data. *J Geophys Res* 100:22047–22070
- Poudjom Djomani YH, Diament M, Wilson M (1997) Lithospheric structure across the Adamawa plateau (Cameroon) from gravity studies. *Tectonophysics* 237:317–327
- Putirka KD (2008) Thermometers and barometers for volcanic systems. *Rev Min Geochem* 69(1):61–120

- Rizzo AL, Faccini B, Casetta F, Faccincani L, Ntaflos T, Italiano F, Coltorti M (2021) Melting and metasomatism in West Eifel and Siebengebirge sub-continental lithospheric mantle: evidence from concentrations of volatiles in fluid inclusions and petrology of ultramafic xenoliths. *Chem Geol* 581:120400
- Rudnick RL, McDonough WF, Chappell BW (1993) Carbonatite metasomatism in the northern Tanzanian mantle: petrographic and geochemical characteristics. *Earth Planet Sci Lett* 114 (4):463–475
- Shemang EM, Ajayi CO, Jacoby WR (2001) A magmatic failed rift beneath the Gongola arm of the upper Benue trough, Nigeria? *J Geodyn* 32:355–371
- Simkin T, Smith JV (1970) Minor element distribution in olivine. *J Geol* 78(3):304–325
- Sun SS, McDonough WF (1989) Chemical and isotopic systematics of oceanic basalts: implications for mantle composition and processes. *Geol Soc London Spec Publ* 42:313–345
- Tamen J, Nkoumbou C, Reusser E, Tchoua F (2015) Petrology and geochemistry of mantle xenoliths from the Kapsiki Plateau (Cameroon Volcanic Line): Implications for lithospheric upwelling. *J Afr Earth Sc* 101:119–134
- Temdjam R (2012) Ultramafic xenoliths from Lake Nyos area, Cameroon volcanic line, West-central Africa: petrography, mineral chemistry, equilibration conditions and metasomatic features. *Chem Erde* 72(1):39–60
- Temdjam R, Boivin P, Chazot G, Robin C, Rouleau E (2004) L'hétérogénéité du manteau supérieur à l'aplomb du volcan de Nyos (Cameroun) révélée par les enclaves ultrabasiques. *Comptes Rendus Géoscience* 336:1239–1244
- Toteu SF (1990) Geochemical characterization of the main petrographical and structural units of Northern Cameroon: implications for Pan-African evolution. *J Afr Earth Sc* 10 (4):615–624
- Toteu SF, Michard A, Bertrand JM, Rocci G (1987) U/Pb dating of Precambrian rocks from northern Cameroon, orogenic evolution and chronology of the Pan-African belt of central Africa. *Precambr Res* 37(1):71–87
- Toteu SF, Van Schmus WR, Penaye J, Michard A (2001) New U-Pb and Sm-Nd data from north-central Cameroon and its bearing on the pre-Pan African history of central Africa. *Precambr Res* 108 (1–2):45–73
- Upton BGJ, Downes H, Kirstein LA, Bonadiman C, Hill PG, Ntaflos T (2011) The lithospheric mantle and lower crust-mantle relationships under Scotland: a xenolithic perspective. *J Geol Soc, London* 168(4):873–886
- Wandji P, Bardintzeff JM, Ménard JJ, Tchoua FM (2000) The alkaline fassaite-bearing volcanic province of the Noun Plain (West-Cameroon). *Neues Jb Min Monat* 1:1–14
- Wells PRA (1977) Pyroxene thermometry in simple and complex systems. *Contrib Mineral Petrol* 62:129–139

Springer Nature or its licensor (e.g. a society or other partner) holds exclusive rights to this article under a publishing agreement with the author(s) or other rightsholder(s); author self-archiving of the accepted manuscript version of this article is solely governed by the terms of such publishing agreement and applicable law.